The new Multi-Frequency Instrument (MFI2) for the QUIJOTE facility in Tenerife

Roger J. Hoyland[a,b], José Alberto Rubiño-Martín[a,b], Marta Aguiar-González[a,b], Paz Alonso-Arias[a,b], Eduardo Artal[g], Mark Ashdown[h,i], R. Belén Barreiro[f], Francisco J. Casas[f], Carlos Colodro-Conde[a,c], Elena de la Hoz[f,k], Mateo Fernández-Torreiro[a,b], Pablo A. Fuerte-Rodríguez[a,b], Ricardo T. Génova-Santos[a,b], Maria F. Gómez-Reñasco[a,b], Eduardo D. González-Carretero[a,b], Raul González-González[a,b], Federica Guidi[a,b,j], Carlos Hernández-Monteagudo[a,b], Diego Herranz[f], Anthony N. Lasenby[h,i], Carlos H. López-Caraballo[a,b], Enrique Martínez-González[f], Asier Oria-Carreras[a,b], Michael W. Peel[a,b], Angeles Pérez-de-Taoro[a,b], Cristina Pérez-Lemus[d], Lucio Piccirillo[e], Rafael Rebolo[a,b], Jesús Salvador Rodríguez-Díaz[a,b], Rafael Toledo-Moreo[d], Afrodisio Vega-Moreno[a,b], Patricio Vielva[f], Robert Anthony Watson[e], and Antonio Zamora-Jimenez[a,b]

[a]Instituto de Astrofísica de Canarias, Calle Vía Láctea SN, ES38205 La Laguna, Spain
[b]Departamento de Astrofísica, Universidad de La Laguna, ES38206, La Laguna, Spain
[c]IAC Technology, Parque Científico y Tecnológico de Tenerife S.A. Calle Rectora María Luisa Tejedor Salguero. Parque Urbano Las Mantecas, Edificio Nanotec, 38320 La Laguna, Spain
[d]Escuela Técnica Superior de Ingeniería de Telecomunicación, Universidad Politécnica de Cartagena, Edif. Antigones, Cartagena, 30202, Spain
[e]Jodrell Bank Centre for Astrophysics, University of Manchester, Oxford Road, Manchester M13 9PL, UK
[f]Instituto de Física de Cantabria (IFCA), CSIC-Univ. de Cantabria, Avda. los Castros, s/n, E-39005 Santander, Spain
[g]Universidad de Cantabria, Departamento de Ingenieria de Comunicaciones (DICOM),Edificio Ingeneria de Telecomunicación. Plaza de la Ciencia nº 1. 39005 Spain
[h]Astrophysics Group, Cavendish Laboratory, University of Cambridge, J J Thomson Avenue, Cambridge CB3 0HE, UK
[i]Kavli Institute for Cosmology, University of Cambridge, Madingley Road, Cambridge CB3 0HA, UK
[j]Institut d'Astrophysique de Paris, UMR 7095, CNRS & Sorbonne Université, 98 bis boulevard Arago, 75014 Paris, France
[k]Dpto. de Física Moderna, Universidad de Cantabria, Avda. de los Castros s/n, E-39005 Santander, Spain.

ABSTRACT

The QUIJOTE (Q-U-I JOint TEnerife) Experiment combines the operation of two radio-telescopes and three instruments working in the microwave bands 10–20 GHz, 26–36 GHz and 35–47 GHz at the Teide observatory, Tenerife, and has already been presented in previous SPIE meetings (1; 2). The Cosmology group at the IAC have designed a new upgrade to the MFI instrument in the band 10–20 GHz. The aim of the QUIJOTE telescopes is to characterise the polarised emission of the Cosmic Microwave Background (CMB), as well as

Further author information: (Send correspondence to R.J.H.)
R.J.H.: E-mail: roger.hoyland@iac.es, Telephone: +34 922 605200
J.A.R-M.: E-mail: jalberto@iac.es, Telephone: +34 922 605200

Galactic and extra-Galactic sources, at medium and large angular scales.This MFI2 will continue the survey at even higher sensitivity levels. The MFI2 project led by the Instituto de Astrofísica de Canarias (IAC) consists of 5 polarimeters, three of them operating in the subband 10–15 GHz, and two in the subband 15–20 GHz. The MFI2 instrument is expected to be a full 2–3 times more sensitive than the former MFI. The microwave complex correlator design has been replaced by a simple correlator design with a digital back-end based on the latest Xilinx FPGAs (ZCU111). During the first half of 2019 the manufacture of the new cryostat was completed and since then the opto-mechanical components have been designed and manufactured. It is expected that the cryogenic front-end will be completed by the end of 2022 along with the FPGA acquisition and observing system. This digital system has been employed to be more robust against stray ground-based and satellite interference, having a frequency resolution of 1 MHz.

Keywords: CMB, Polarimeter, FPGA, early Universe, microwaves, telescopes, instrumentation, cryogenics, direct digital conversion

1. INTRODUCTION

The Q-U-I JOint Tenerife Experiment (QUIJOTE, 3) is a scientific collaboration between the Instituto de Astrofisica de Canarias (IAC), the Instituto de Fisica de Cantabria (IFCA), the Universities of Cantabria, Manchester and Cambridge, and the IDOM company, with the aim of characterising the polarisation of the cosmic microwave background (CMB) and other Galactic and extragalactic physical processes in the frequency range 10–40 GHz and at large angular scales ($\sim 1^\circ$). It consists of two identical telescopes, QT-1 (4) and QT-2 (5; 6), equipped with several instruments. The QUIJOTE telescopes are based on an offset crossed-Dragone design with projected apertures of 2.25 and 1.89 m for the primary and secondary mirrors respectively, which provides optimal polarisation properties. QT-1 is focused on observations at low frequencies (10–20 GHz), and was operating between 2012 and 2018 with the Multi-Frequency Instrument (MFI, 2; 7).From 2018-2020 the KISS spectrometer was mounted(KISS, 8). QT-2 is dedicated to observations in the 30–40 GHz range, using two instruments, the Thirty-GHz Instrument (TGI) and the Forty-GHz Instrument (FGI) (7). Both TGI and FGI share the same cryostat, which contains space for 29 detectors ("pixels") that can be reconfigured in multiple ways. At the moment, we are observing in a configuration with pixels at both 30 and 40 GHz, which we call TFGI.

QUIJOTE is located at the Teide Observatory (2,400 m above sea level) in Tenerife (Canary Islands), a site with excellent observing conditions for microwave observations (median pwv of 3.5 mm, see 9), and with a long tradition of more than 35 years in CMB research. In addition to QUIJOTE, there are three CMB experiments that are either running at the moment, or to be installed in the next year: GroundBIRD (10), LSPE-STRIP (11), and the Tenerife Microwave Spectrometer (TMS, 12).

QUIJOTE has a primary science goal: to provide essential information of the polarisation properties of the synchrotron and anomalous microwave emissions from our Galaxy (3). Regarding the second goal, QUIJOTE MFI provides unique information in the frequency range 10–20 GHz, a band that complements at low frequencies the existing maps from WMAP (13) and Planck (14) satellites, and that is not covered by any other CMB experiment at the moment. With the initial and future instruments a further goal is to detect the imprint of primordial gravitational B-modes if they have an amplitude of $r \geq 0.05$. MFI was operative on the focal plane of the QT1 from November 2012 to August 2018. During this time it accumulated 25,000 hours of data, out of which approximately 10,000 h were invested in a wide-survey of the full northern sky (29,000 $\deg^2$) at 11, 13, 17 and 19 GHz. The resulting MFI wide-survey maps have sensitivities of approximately 45 μK/deg in polarization (see Fig 1). These are the first polarisation maps ever obtained over such a large sky fraction in this frequency range, and thence will have an important legacy value to correct future CMB experiments from galactic foregrounds. The MFI maps will be made publicly available during 2022 (15).

The importance of having observations in this low frequency range as a legacy for future B-mode missions has been recognised by the CMB community (see e.g. 16; 17). Because of this reason, from the QUIJOTE collaboration we are finalising now a new version of the MFI, the MFI2, which will have an improved sensitivity by a factor of 2–3, and will incorporate technological improvements that will allow better removal of the radio interference (RFI). MFI was decommissioned in 2019. This paper describes in detail this new MFI2 instrument for QUIJOTE.

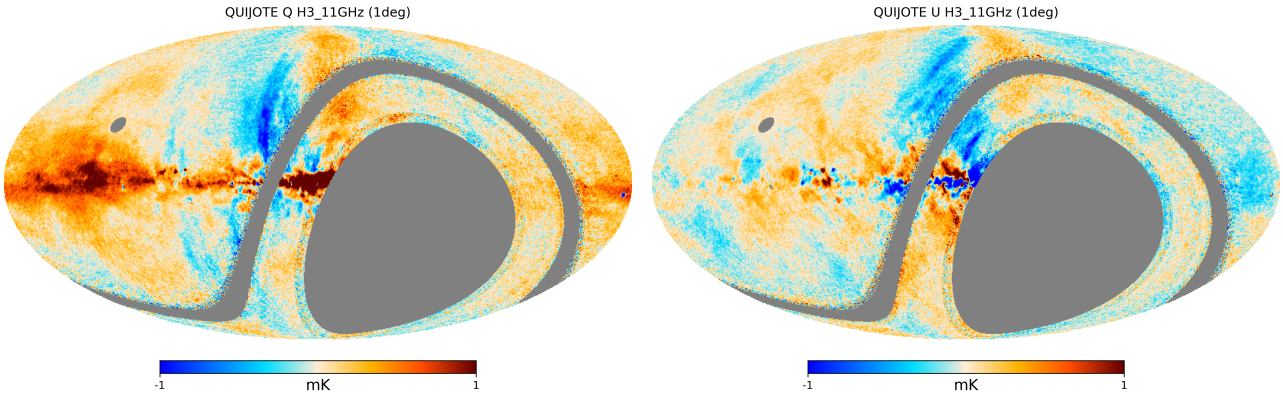

Figure 1: Polarization maps at 11 GHz (Stokes Q on the left, Stokes U on the right) of the full Northern hemisphere (declinations above $-30°$) obtained with the MFI instrument on the QUIJOTE telescope (from around 10,000 hours of observations). These maps clearly show both diffuse emission from our Galaxy, as well as compact emission from bright synchrotron-emission regions, and are unique as they are the first ever obtained in these frequencies and over such a large sky area. The unobserved band around declination zero degrees is due to the emission of geo-stationary satellites. Figure taken from (15).

2. SCIENCE GOALS AND TOP-LEVEL REQUIREMENTS

MFI2 keeps and extends the scientific goals of the former MFI instrument, which were focused on the characterisation of the polarisation properties of the Galactic synchrotron and anomalous microwave emission (AME) (see details in Sect. 4 of 3). The top level scientific requirements of the MFI2 instrument are:

- the improvement of the raw sensitivity of the former MFI by a factor of 2–3. This will allow us to conduct a new MFI2 wide survey targeting a sensitivity of 15 μK/deg at 11 GHz, which is equivalent to 1 μK.arcmin at 100 GHz for a synchrotron-like spectrum with $\beta = -3.1$.
- to implement the ability for RFI removal in the new version of the instrument.

The first goal will be achieved by a huge simplification of the opto-mechanical design of the instrument, which now will not use motors and polar modulators. In addition, state-of-the-art cryogenic amplifiers will significantly improve the system temperature of the new instrument. For the second goal, as explained in (15), the main source of systematic effects in the MFI wide survey is the emission of geo-stationary satellites, both direct emission and the signals appearing through the far sidelobes. Direct emission from satellites prevented us from observing the band around declination zero (see Fig. 1), while the presence of RFI signals seen in far sidelobes was corrected using a large-scale filter which removes a constant mode for those pixels in the map with the same declination. MFI2 should have the capability to filter out these unwanted RFI signals, thus allowing us to recover all angular scales and extend the observable sky area.

Moreover, the situation with RFI emissions in this frequency band is expected to become worse with time. Satellites actively transmit at the frequencies that MFI2 will observe at, and cannot be avoided by being located on a remote site such as Teide Observatory. In addition to the geostationary satellites, which form a bright Ku-band chain of satellites around declination 0°, we will have also low earth orbit satellites that quickly move across the whole of the sky. Since MFI stopped observing in 2018, thousands of LEO communication satellites have been launched, particularly by Starlink, and need to be mitigated. This cannot be done using broadband detectors, instead, digital back-ends are required to reject satellite interference and preserve as much bandwidth as possible for astronomical observations. Figure 2 shows approximately one hour of data showing the frequency usage of the 250 MHz bands for the Starlink and OneWeb satellites within the allocated band of 10.7 to 12.7 GHz.

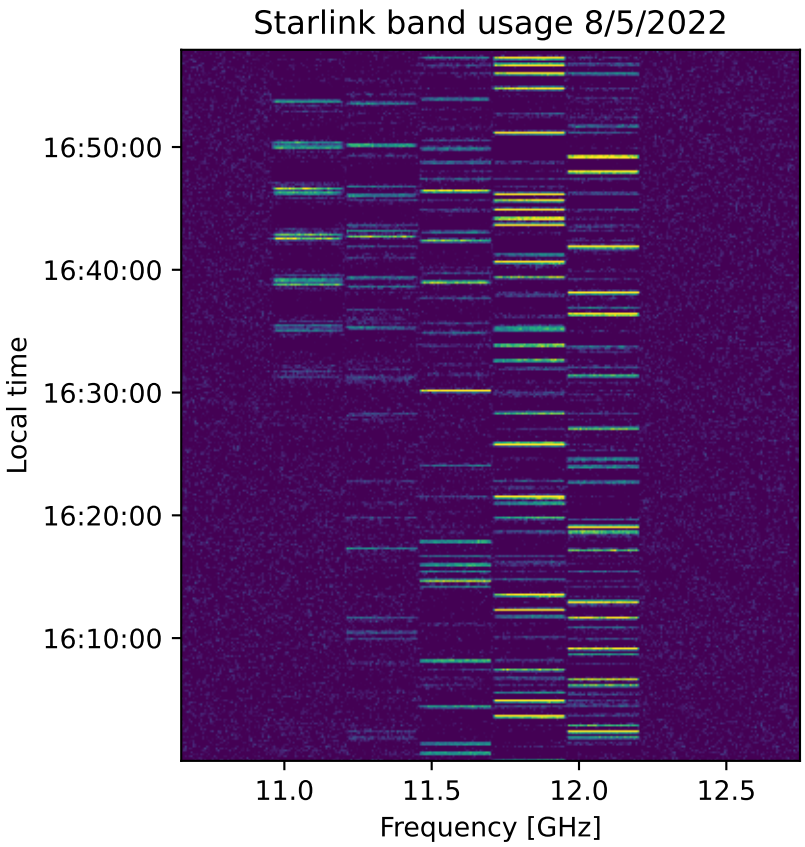

S

Figure 2: Approximately one hour of data showing the frequency usage of the 250 MHz bands for the Starlink and OneWeb satellites within the allocated band of 10.7 to 12.7 GHz.

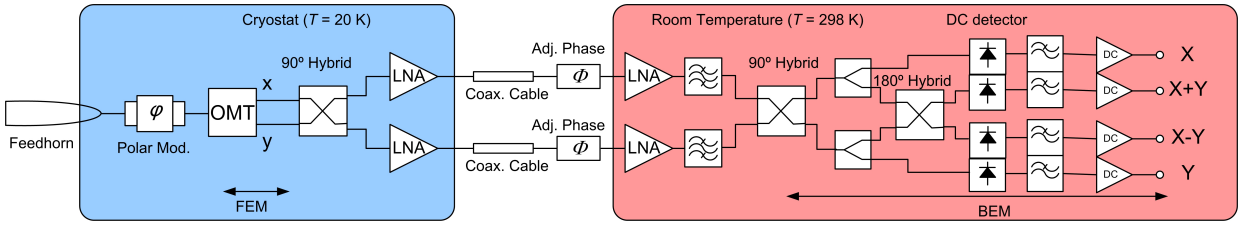

Figure 3: The pseudo-correlation approach used for the design of the MFI radiometer. In *blue* background, we represent the first stage, cooled to < 60 K, with the ultra-LNAs and hybrids at 20 K. In *red*, we represent the Back-End Modules (BEM) in the second stage, kept at room temperature. The BEMs include a warm gain stage and bandpass filters followed by another hybrid to decorrelate the signal passing through the two arms. The outputs from the OMT are voltage linear polarisations, x and y. These are correlated through 90° couplers. Finally the output is decorrelated and split into 4 with a further hybrid combining the two central outputs. In this way the 4 outputs give an equivalent amplitude (power) to X,X+Y,X-Y,Y Linear polar outputs

3. THE MFI2 DESIGN SCHEME

3.1 The Optimum MFI scheme

During its 6 year observation period from November 2012 – October 2018, the MFI has undergone several modifications in order to fulfill its design goals. Figure 3 shows a schematic diagram of the final configuration

employed in the instrument. The MFI was originally designed to make polarisation observations with a constantly fast spinning (10 Hz) cold polar modulator just after the feedhorn. This technique was shown to work taking various moon observations but only rotating the polar modulator at a frequency of 1 Hz. This was due to the uncontrollable heating through the polar modulator cryo-bearings for fast spin rate. Due to the need for long term reliability it was decided that the modulator should be stepped every so often rather than spun continuously. This changed the observational strategy and instrumental scheme. A pair of 90° hybrids had to be added either side of the gain stages so as to correlate the X,Y signals through both arms, and to separate them at the output, each having undergone identical 1/f gain modulation. The polar modulator now serves to extract systematic errors in the polarimeter rather than its original design to switch polarisations between the outputs faster than the 1/f knee frequency.

The MFI design is not optimum in its present state. The polar modulator, designed for fast rotation, puts a large thermal load on the system and raises the physical temperature at this point to about 50–60 K even when it is stationary. Now that it is only used for systematic error removal it is not regarded as essential to the design and can be removed, thus allowing the FEMs to be cooled to < 20 K physical temperature. Low Noise Factory* has brought out a new run of 6–20 GHz cryogenic LNAs that halve the average noise temperature across the band compared to the previous model used in the MFI. These will be employed in the MFI2. The MFI focal plane also only used 4 out of the possible 5 pixel positions since a high frequency channel of 26–36 GHz was ultimately not employed in the MFI. In the MFI2 all the 5 pixel positions will be used, the central pixel being occupied by a 10–15 GHz polarimeter. Finally, the observable bands for MFI were 10–14 GHz and 16–20 GHz. The central 14–16 GHz band was eventually discarded due to a significant interference from the Teide Observatory microwave backup link up from sea level. There was no easy way of avoiding the 14.5–15.3 GHz interference without removing a large percentage of the band. The MFI2 will observe across 4 subbands, 10–12.5 GHz, 12.5–15 GHz, 15–17.5 GHz, 17.5–20 GHz with the idea of removing specific interference with the high fidelity digital back-end.

3.2 Improvements implemented in the MFI2

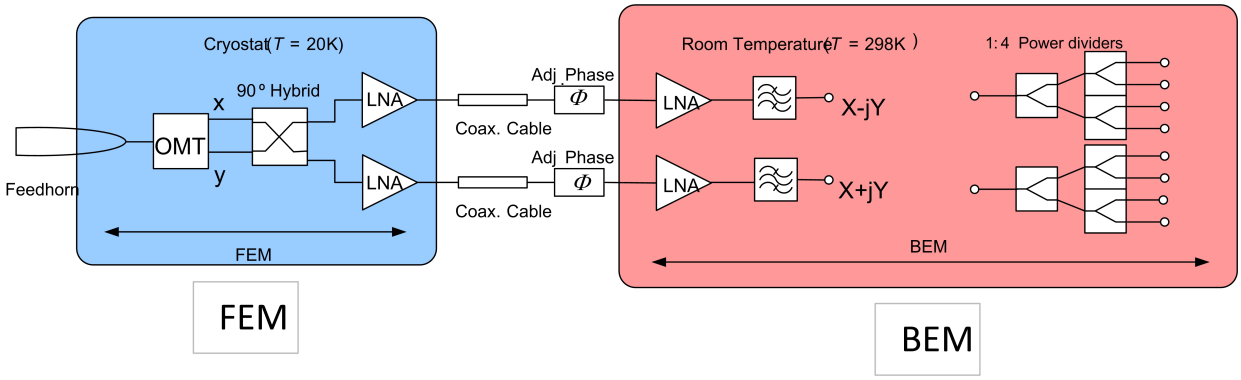

Figure 4: The simplified digital correlator approach to the MFI2. In *blue* background, we represent the first stage, cooled to 20 K, with the simplified Front-End Modules (and no polar modulator). In *red*, we represent the Back-End Modules in the second stage, kept at room temperature. Only the warm gain blocks and diplexer array are shown. The down-conversion stage is not included in this representation.

Figure 4 shows the schematic diagram of the new MFI2 polarimeter design. It can be seen that the modules have been significantly simplified at the cost of complicating the downconversion and digital backend. The cold cryogenic module now only houses the throat of the feedhorn, the OMT, 90° hybrid coupler and two commercial (Low Noise Factory) cryogenic LNAs (LNF_LNC620_C†) . The simplified design allows the cryostat to cool to

*https://lownoisefactory.com

†https://lownoisefactory.com/product/lnf-lnc6_20c/

$< 20\,\mathrm{K}$ physical temperature, increasing the overall sensitivity of the receiver. The cryogenic module is connected to the BEM via long coaxial cable runs with the first element encountered being a commercial LNA. The two arms of the polarimeter are then fed into a custom built diplexer array which divides the band up in to its 4 subbands ready for distribution to the downconverter blocks. The array ensures complete coverage of the full band without overlap or gap, which is an improvement on the MFI. In total there are 10 such diplexer arrays which are identical and optimise reuse and board replacement for this project. They are made in-house using SMT components mounted on Rogers Duroid 5880 PCB[‡].

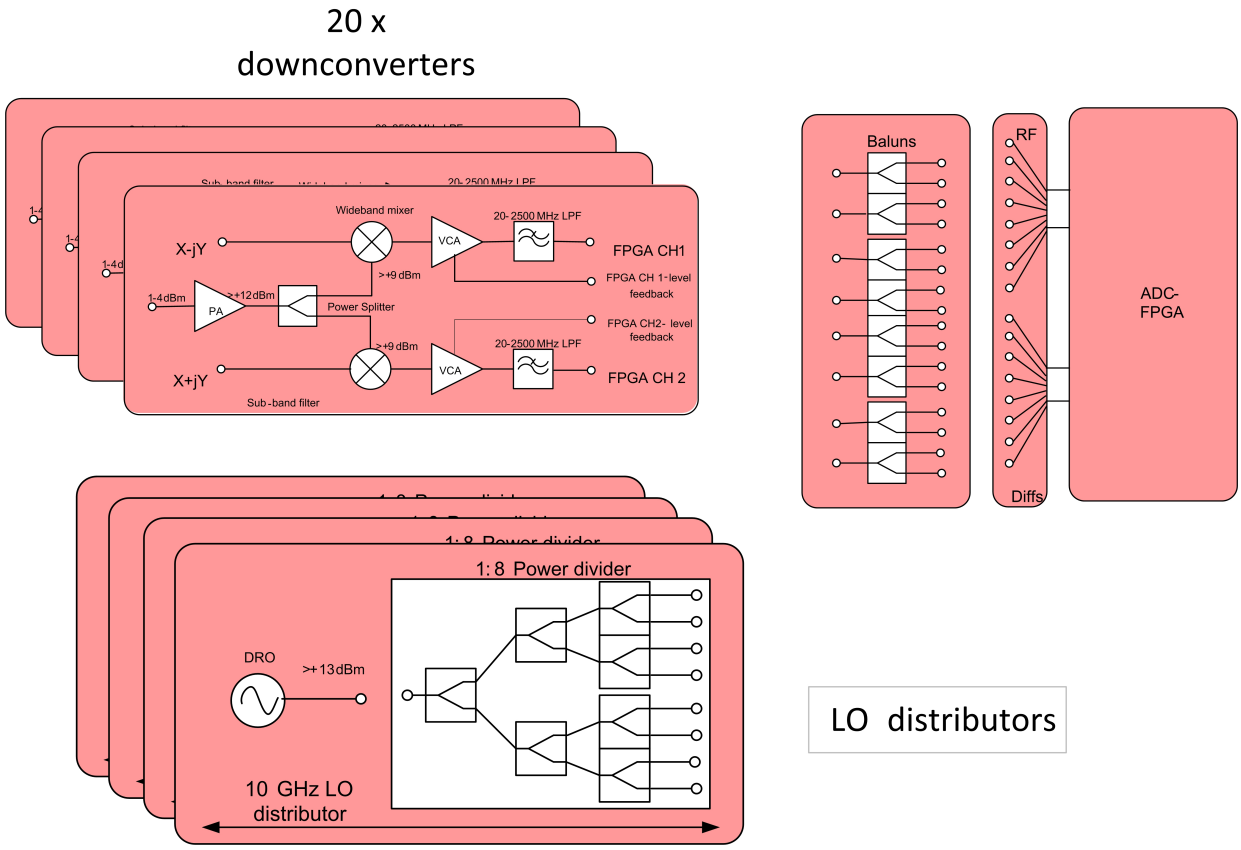

Figure 5: A schematic diagram of the MFI2 downconversion and LO distribution blocks. To complete the MFI2, 4 LO distribution blocks and 20 downconverters are needed.

Figure 5 shows a schematic diagram of the downconversion and FPGA preconditioning modules. For the MFI2 array there is need of 20 downconverters and 4 LO distribution modules for the 5 pixel array. The design has been optimised for circuit reuse and ease of in-house manufacture as well as cost effectiveness. The components have been procured as a mixture of packaged, SMT packaged and pcb mountable modules from several commercial companies such as MINI-CIRCUITS[§] and Markimicrowave[¶]. The LO distribution module is designed to distribute the 4 LO frequencies (10 GHz, 12.5 GHz, 15 GHz, 17.5 GHz) to each of the corresponding downconversion modules. The packaged SMA LO outputs are $+13\,\mathrm{dBm}$ and this is divided into 8 SMA outputs via an in-house divide-by-8 PCB. The routing of the LO signals is through equi-length semi-rigid cable. The downconverter modules receive this input (now at $+13-9 = +4\,\mathrm{dBm}$) and amplify the signal through a broadband SMT power amplifier with 10 dB gain. The resulting signal is divided in equal phase between 2 broadband mixers. Meanwhile each downconverter card receives two output pairs from a given pixel BEM to the mixer RF inputs.

[‡] https://rogerscorp.com/
[§] https://www.minicircuits.com
[¶] https://www.markimicrowave.com/home

The mixer outputs then pass the downconverted signal through a low frequency amplitude gain control (AGC), which is a combination of a PA and digitally controlled attenuator. Finally the signal passes through a 2.5 GHz low pass filter before passing on to the FPGA input. The FPGA input consists of a set of baluns to convert the standard 50 ohm single-ended input into a balanced output through a PCB mountable coil design from MINI-CIRCUITS. It is foreseen that each PCB will be housed in a purpose-built aluminium box as is used in good RF design with the SMA connectors and semi-rigid cable providing a solid coaxial interconnect between each box.

3.3 The digital FPGA based backend

Field programmable gate arrays (FPGAs) present a great advantage over other kind of back-ends due to the digital processing capability on the actual microwave signal. Critical microwave BEM components such as the phase switch and wide-band hybrid are eliminated and replaced by mathematical processing hard-wired in the FPGA. The bandwidth limitation of FPGAs has been greatly improved these last few years (mostly because of a great interest for many industrial applications) and now the latest FPGAs offer a 2.5 GHz direct input and processing capability. This is sufficiently wide to provide a simple band-splitting and down conversion system for our 10 GHz band. One FPGA can manage 8 channel parallel inputs, which means that one FPGA can be used per pixel, which offers overall low power consumption and efficiency in the use of resources (parallel computing architecture). Of course, until recently FPGA-based spectrometers were not particularly common, partly due to the complex programming using Hardware Description Language (HDL) and maintenance of FPGA systems but mainly because of their limited bandwidth. Nowadays, new tools have made FPGAs more accessible and easier to program, verify and maintain, not only for the industry but also in other applications such as instrumentation for radioastronomy[‖]. In this field, they can offer a solution for real-time broadband operation and a spectral resolution capacity of thousands of channels. With all these possibilities the FPGA solution provides an obvious choice for the MFI2 BEM. This digital solution will allow a high resolution template based spectral filter to be implemented to reject the possible RF interference in the band. These are the main reasons, behind the selection of a FPGA-board for the implementation of an ultra-fast acquisition system and RF interference robust system, despite the increased complexity of the design in other areas and added cost.

The MFI2 FPGA, ZCU208, will implement a hard programmed polyphase filterbank (PFB) and a Fast Fourier Transform (FFT) in order to retrieve the spectral information from the digitised samples of the fast onboard ADCs in the time domain. Figure 6 shows the scheme for this implementation. A graphical description of the PFB operation is shown below. A $M \times P$ buffer is used to store the time samples for each cycle. The sequential switch splits the input into the P filterbank branches, feeding the P polyphase filters. Each filter presents M taps or coefficients used for weighting the incoming data. The polyphase filter operation can be expressed as

$$y[n] = \sum_{p=0}^{P-1} \sum_{m=0}^{M-1} h_p[m] x[n-m] \tag{1}$$

where $h_p[n]$ represents the weighting coefficients of the digital filters, usually based on the Hamming and Hann windowing functions (see Fig. 7).

PFBs present two attractive features for the MFI2 FPGA acquisition system. First, the MFI2 FPGA acquisition system must simultaneously acquire and deal with four 2.5 GHz signals giving a total of 10 GHz bandwidth and their channelisation, with a very strict requirement on synchronisation. The PFBs parallelised structure is well suited for implementations on FPGA-chips, whose strength is its parallel computing architecture. The fast hard-wired on-board processing means that the output rate is more manageable since the temporal integration of the signal is achieved in the FPGA. The digital acquisition system (DAS) digitises the radiometer output signals, and conditions and pre-processes them by filtering and correcting radio interferences. The MFI2 DAS system—currently under development at the IAC—is based on a System-on-Chip Field Programmable Gate

[‖]The Collaboration for Astronomy Signal Processing and Electronics Research (CASPER, https://casper.berkeley.edu/) has given easy access to open source resources, libraries and tools that can be used to implement and design spectrometers for (radio) astronomical instrumentation.

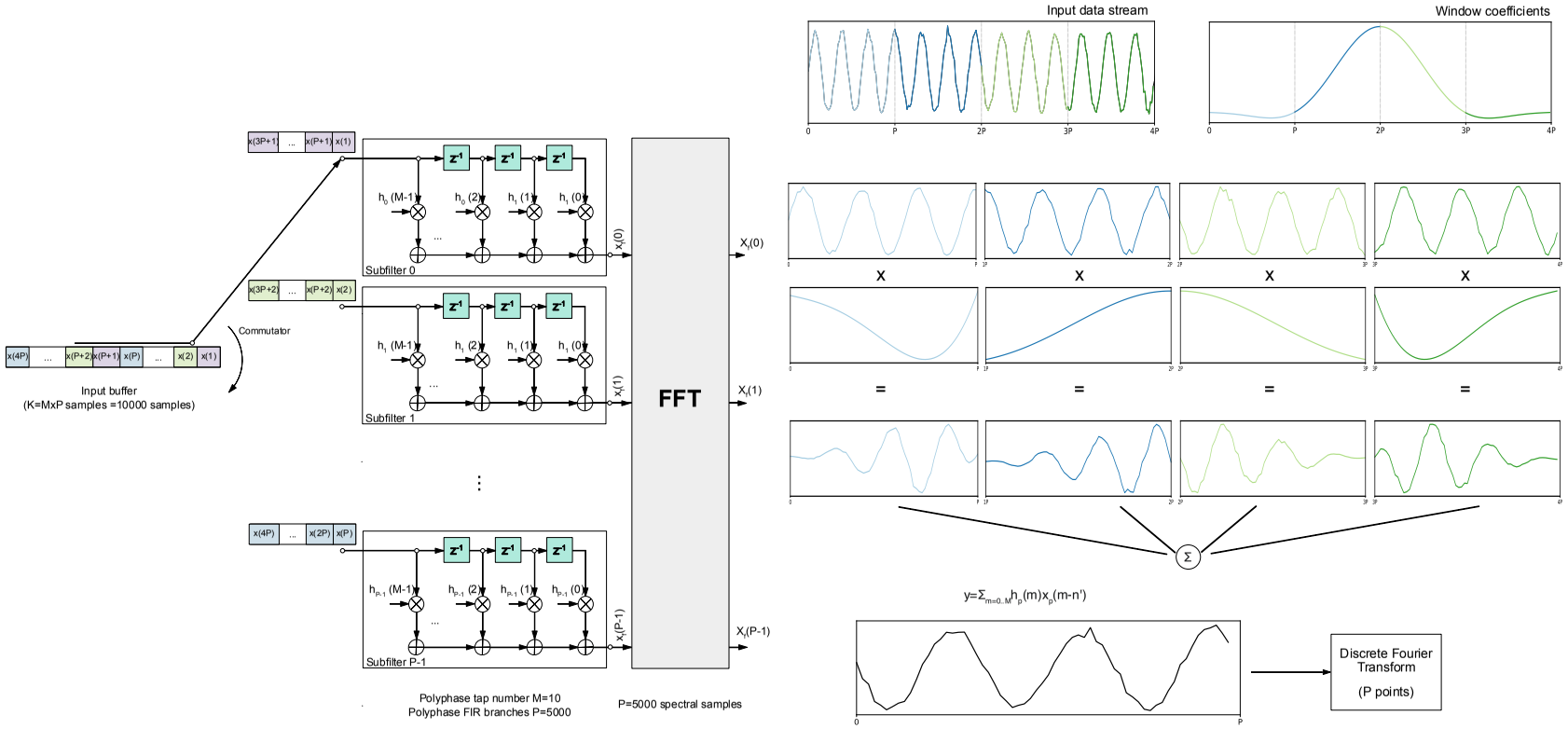

Figure 6: Polyphase FIR filterbank and Fast Fourier Transform architecture (PFB). Images adapted from (18). *Left:* PFB+FFT architecture scheme. Indices m and p, running from 0, denote the filter tap and FIR filter, respectively. For the MFI2 FPGA-chip, we will implement P=5000 FIR filters with M=10 taps. A colour code has been used in order to clarify the operation of the PFB. Number of spectral samples at the output of the system is P=5000. *Right:* Graphical representation of a PFB and FFT with P=64 and M=4. Input samples are temporarily stored in a buffer of $M \times P$ samples. The data (*top, left*) and filter coefficients (*top, right*) are multiplied together, split in M taps, and then added. Finally, the P-point FFT is computed.

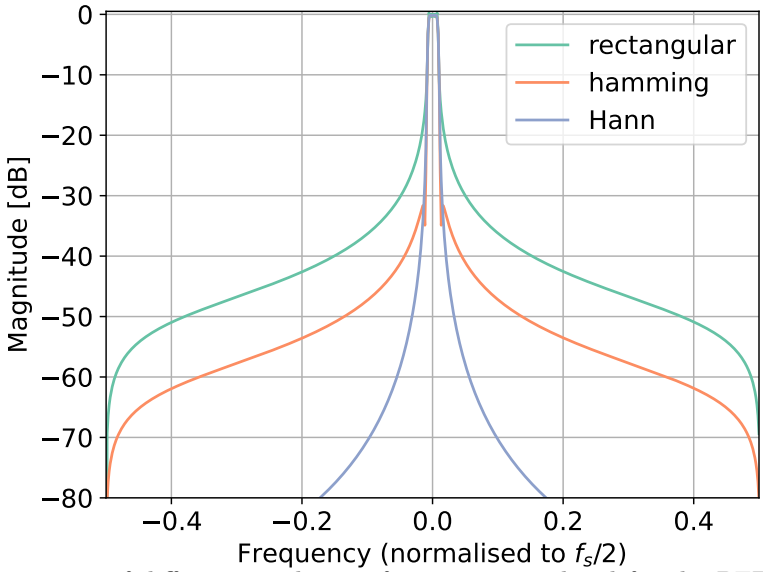

Figure 7: Spectral response of different windowing functions considered for the PFB implementation. With a rectangular window (*green* colour, all samples are weighted equally. This is the case that provides the worst isolation between bands. Hamming and Hann windowing functions (in *orange* and *violet*, respectively) reduce the effect of adjacent bands, providing isolation of up to 60 dB.

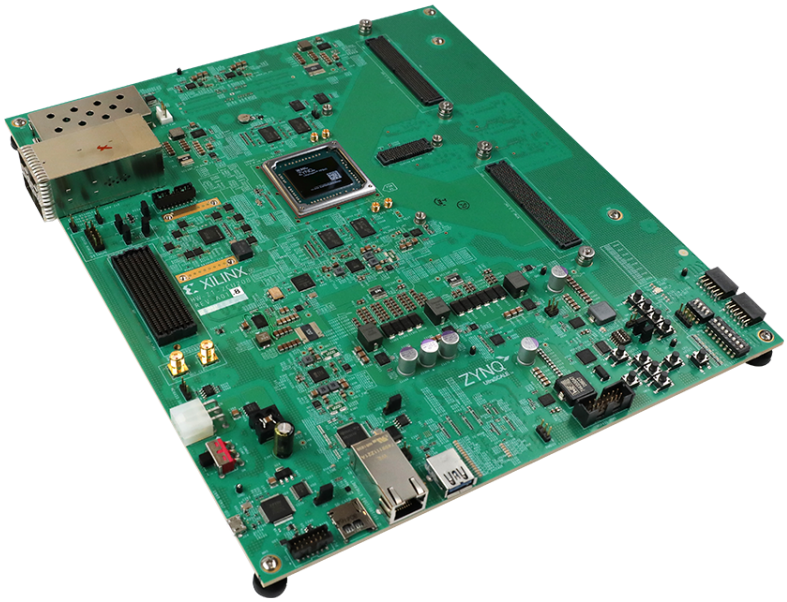

Figure 8: Angled view of the ZCU208 RFSoC Ultrascale board from Xilinx

Array (SoC-FPGA), as they provide high resolution, fast acquisition, real time signal processing and control, and allow several modes of operation. It will be implemented using the Xilinx ZCU208 Ultrascale (see Fig. 8), which has the capability to simultaneously acquire eight RF channels at a sampling frequency of 5.0 GSps. To implement this, the two outputs of each radiometer band will be divided into 4 spectral subbands with maximum bandwidth of 2.5 GHz down-converted to base band by means of the down-conversion modules previously explained. The MFI2 DAS system presents two modes of operations: in the engineering mode, the system will operate with one or two RF channels, and will allow us to verify the correct behaviour of the SoC; in the science mode, the system will operate continuously performing complete observations.

The FPGA acquisition system scheme is graphically described in Fig. 9. The implementation presents a modular architecture with five main signal processing blocks: the analog to digital converter (ADC), the polyphase finite impulse response (FIR) filterbank and Fast Fourier Transform block (FFT), two blocks of linear and nonliner combinations to reconstruct the Stokes parameters spectra, and the accumulator to perform the averaging of the rebuilt signals. Each input signal and subband receives the same treatment in parallel and thus, for the sake of simplicity, the scheme includes the acquisition and processing of one single RF input channel.

The sampling frequency is 5.0 GSps, establishing a maximum bandwidth of 2.5 GHz at each RF input. A complete down-conversion module has been designed to divide the MFI2 operational band into the required number of RF inputs. The acquisition system digitises the 20 RF input channels[**], and routes the *raw* data into the FPGA in parallel. For each branch, the FPGA stores the digital samples in a buffer before forwarding it to a polyphase finite impulse response (FIR) filter bank. Four parallel polyphase FIR filterbanks and FFT are implemented for each 2.5 GHz subband, resulting in a total of 16 filterbanks and FFTs running in parallel. The polyphase filterbank and FFT blocks allows the reconstruction of the spectra of the input signals, ensuring the preservation of phase information, and providing high-isolation between subbands.

Once the spectral information is retrieved, the spectral samples of each RF subband, with frequency sampling of 1 MHz, are linearly combined in order to decouple the sky and load signals and reconstruct the Stokes parameter spectra in the whole MFI2 band. In addition, the four subband spectra, still in the 0–2.5 GHz frequency range, are then arranged to reconstruct the spectrum in the original band between 10–20 GHz. Then, the square modulus of each Stokes spectra is calculated and accumulated during an averaging cycle of 1000 iterations. The averaged set of data is forwarded to the external PC. In the science mode, the system will operate continuously performing complete observations. Data will be sent at an output rate of no less than 0.5 Gbps (matching the FPGA output rate) to be stored on a SSD. This communication will be achieved by means of the standard Ethernet protocol using SFP optical interface modules operating at 10 Gbit/s. Recent SSD array incorporate direct Ethernet connection and can be "hot-swapped" if necessary. As a first estimation for the storage solution this SSD array will be placed in the QUIJOTE telescope building having the capacity to store 1 month of raw data. During this time the interference template filter will be optimised for each observation so that the data can be reduced correctly. From the estimated data flow described here there will be need of an SSD array of size 5 × 162 Tbytes SSDs. The reduced data which will offer a 250 MHz sub-band every 4 ms will produce 5 × 162 Gbytes of data per month. These SSDs must support continuous write/read at the data input and output rate. The data will be read by a local computer and reduced so that it can be transferred and stored on the IAC safe storage system for further post processing.

4. THE EXPECTED PERFORMANCE IMPROVEMENT

4.1 Noise performance

Table 1 gives a comparison of the expected noise parameters of the MFI2 instrument and the old MFI. The contributions from each significant noise source are included (CMB, sky, spillover, optomechanical, LNA, etc.). The number of pixels and equivalent 2 GHz channels are also counted. A final comparison of the noise temperatures is given and also the r.m.s. noise expected at the output per GHz and second. Whereas the noise temperature and r.m.s. noise give approximately 2 fold improvement, the number of channels (and spectral resolution) has increased from MFI to MFI2. Taking into account the superior ability of MFI2 to reject narrow band RF interference we estimate a factor 2–3 improvement in the sensitivity of MFI2 over MFI.

[**]For each FPGA, there are 4 RF channels. MFI2 will use five FPGA cards in order to digitise and process a total of 20 channels. This leaves room for a future upgrade in which the RF bandwidth is 10GHz per pixel

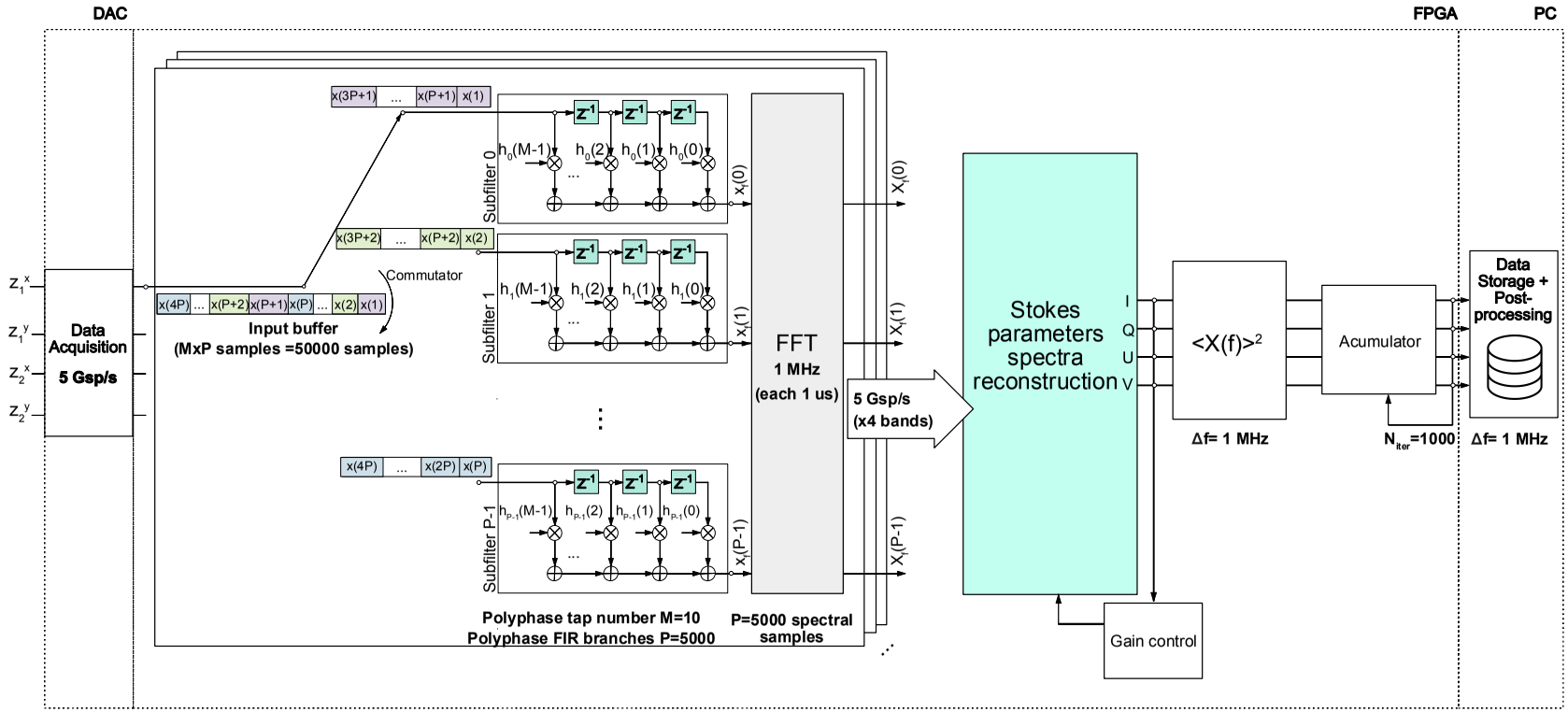

Figure 9: Block diagram of the FPGA-based processing system and offline post-processing for the MFI2. Example of operation for a single RF channel. Output rate of the FPGA is 0.5 Gbps. Five main modules are needed in order to recover the full signal spectrum between 10–20 GHz: the analog to digital conversion (ADC) module, a set of digital filterbanks and Fast Fourier Transform (FFT) blocks, the linear operations to reconstruct the full Stokes parameters spectra, and the power calculation and averaging blocks. The stored I, Q, U, V spectra are resolved with a frequency sampling of 1 MHz, which will be post-processed in order to obtain the final number of spectral points for each time sample (1 ms).

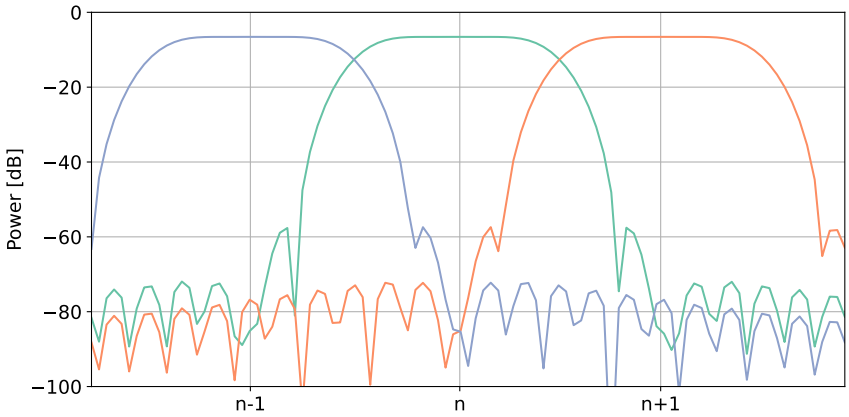

Figure 10: Visualisation of adjacent channels in the PFB implementation using a hamming window filter. Image adapted from (18).

Table 1: Comparison of the present MFI and the new MFI2 noise temperature parameters.

Instrument	MFI	MFI2
No of pixels	4	5
bandwidth	4 GHz	5 GHz
CMB	2.73 K	2.73 K
Sky	5 K	5 K
Spillover	3 K	3 K
Optomechanical	10 K	1 K
LNA NT	9 K	4 K
BEM	5 K	1 K
Overall NT	35 K	17 K
No of 2GHz channels	(2 + 2) x 2	(2+3) x 3
NEP per pixel (2 GHz band)	0.54 mK $s^{1/2}$	0.22 mK $s^{1/2}$

4.2 Interference rejection and bandpass recovery

The MFI2 will operate in a frequency band that is shared with satellite-based communication systems (X and Ku bands). Strong radio frequency interference (RFI) can mask the signal of interest in adjacent channels, especially in the case of astronomical signals, which are typically much fainter. One of the functions of the MFI2 spectrometer block is the minimisation of the effect of satellite interference. While we cannot avoid the contamination of certain pixels in the sky map, we can reduce the effect of RFI to a smaller number of frequency sub-bands, and avoid leakage in nearby bands[††]. The application of a hamming window filter before the FFT computation allows us to minimise this spectral leakage. In Fig. 10, we show adjacent channels and the final isolation achieved by using a polyphase filterbank before the FFT operation. It is yet to be seen just how much of the band can be recovered in MFI2 compared to MFI. The new Starlink constellation will be a challenge due

[††]As a reference, a typical system transmitting in the Ku-band is ASTRA (https://astra.com/), a system of geostationary communication satellites used for digital television broadcasting. The ASTRA satellites operate with bandwidths of 26 MHz. Thus, only 26 1 MHz- subbands would be compromised during the transit of a satellite of the ASTRA constellation.

to its dynamic nature and the geo-stationary satellites may be too bright to recover the pixels close by due to the leakage. However, the MFI2 is in a far better position to take on this task compared to the MFI.

5. THE PRACTICAL IMPLEMENTATION

5.1 The cryostat and cryogenic implementation

The thermal layout of the cryostat consists of three stages separated by anti-radiation shields (Vacuum deposited Aluminium coating). Each stage of the cryostat is connected to the respective stage of the cryocooler by copper thermal links. Furthermore, there are flexible thermal links, which connect the second stage of the cryocooler with the ultra-LNAs directly to compensate for the heat produced by the electrical supply. Each of the feedhorns is also connected to the second stage. In order to minimise conductance heat losses, G10 bars have been used to structurally support the system. The surfaces of the feedhorn are protected by anti-radiation shields at both cryogenic stage levels. Just the throat of the feedhorns are exposed to the radiative heat flux coming from the Mylar viewports. The section of the feedhorn is shown along its length in Fig. 11. As the feedhorn is divided

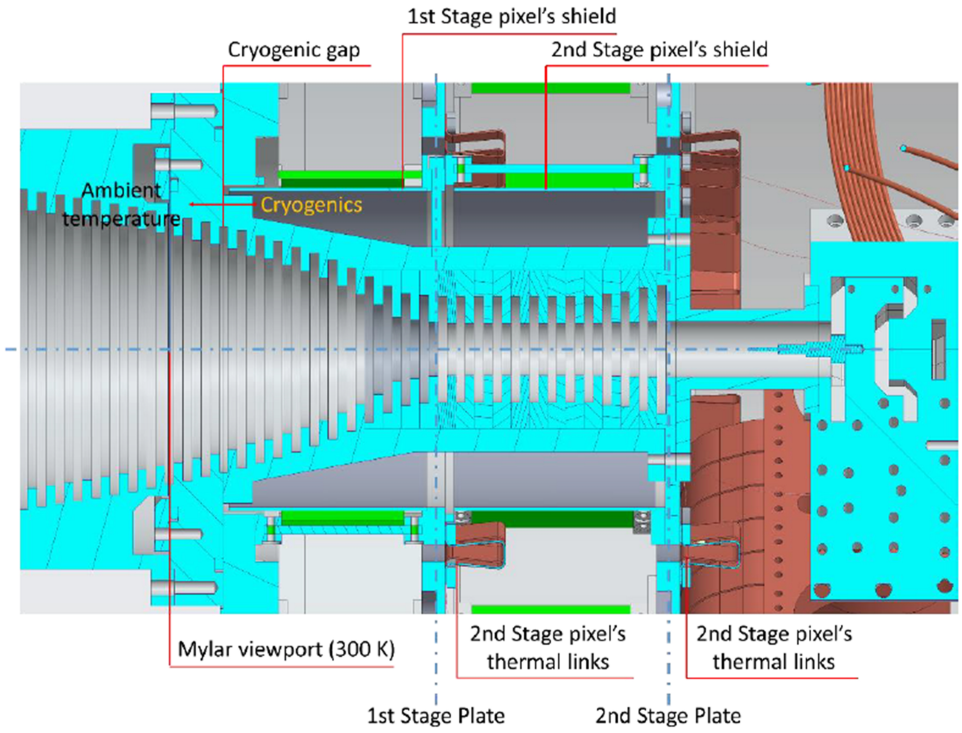

Figure 11: Feedhorn's mechanical scheme

into an ambient temperature external part and a cryogenically cooled one, a thermal gap with a nominal size of 100 μm at ambient temperature separates both parts. When the thermal steady-state is reached, the gap size is 500 μm, which will avoid conductance thermal losses without compromising performance. The cryogenic wiring (ultra-LNA bias wires and coax wires) are connected to a cold board located at the second stage plate. From there, the wires go through a hole located near the plate, making contact with the first stage plate and going to its respective feedthrough connectors. In this manner, the wiring can exit the second stage enclosure without breaking the continuity of the second stage anti-radiative shield (see Fig. 12). To reach at least 20 K as the operation temperature of the ultra-LNA we have employed the Leybold COOLPOWER 10 MD. The operating point is near to 10 K, 2.7 W at second stage and 50 K, 33 W at first stage. The capacity map is shown in Fig. 13[‡‡]. In order to study the temperature distribution of the instrument, steady-state FEM thermal analyses have been

[‡‡](https://www.johnmorrisgroup.com/coolpower-10-md), 240.00.02 Excerpt from the Leybold Full Line Catalog 2016 Catalog Part High Vacuum Pumps Edition: Fall 2016

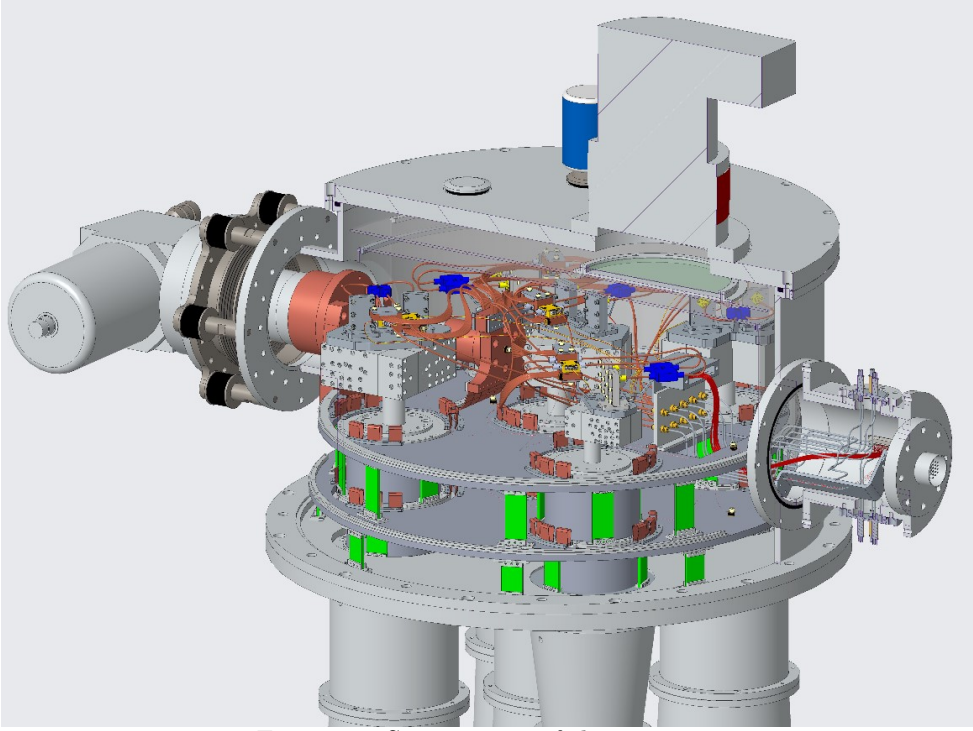

Figure 12: Section view of the cryostat.

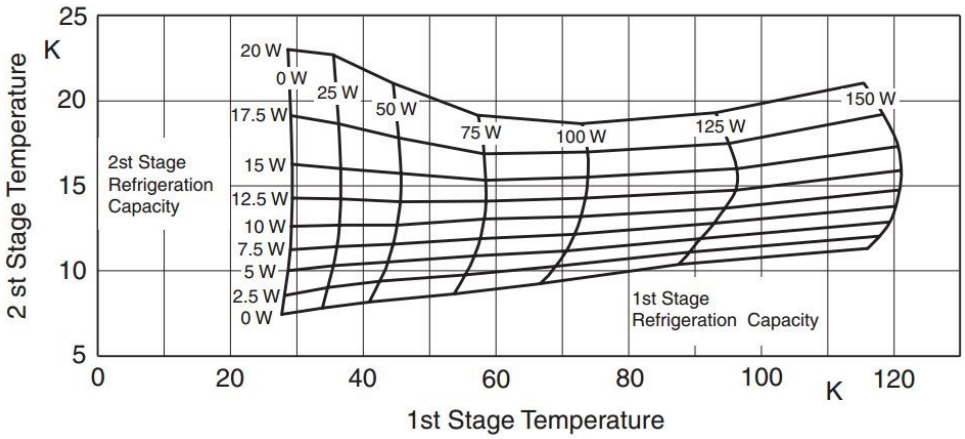

Figure 13: Capacity map of the Leybold COOLPOWER 10 MD used for the MFI2.

performed. Fig.14 shows the second stage temperature distribution. At the time of writing this article, the instrument is under mechanical integration (Fig.15). The cryogenic part of the feedhorns has been assembled and aligned and the size of the thermal gap has been verified at room temperature.

5.2 The overall system organization

Fig. 16 shows the signal and data flow through the complete data acquisition system. The flow starts at the MFI2 cryogenically cooled instrument, which is mounted at the focal plane on the QT1 Quijote telescope. The RF output from this instrument is passed to the downconversion and band separation unit in the BEM where the signal is prepared for the FPGA input. The signal now passes through the 5 FPGA cards in parallel providing 5 digital outputs. With a resolution of 1MHz and a band of 5 GHz with data rate of 1000 samples/s the output per pixel is 20 MS/s or 80 Mbytes/s. For each channel this will give about 640 Mbits/s (with TCP overheads) and a total of 3.2 Gbits/s throughput fed into a 10 Gbit/s ethernet switch. The fibre optic output of the switch

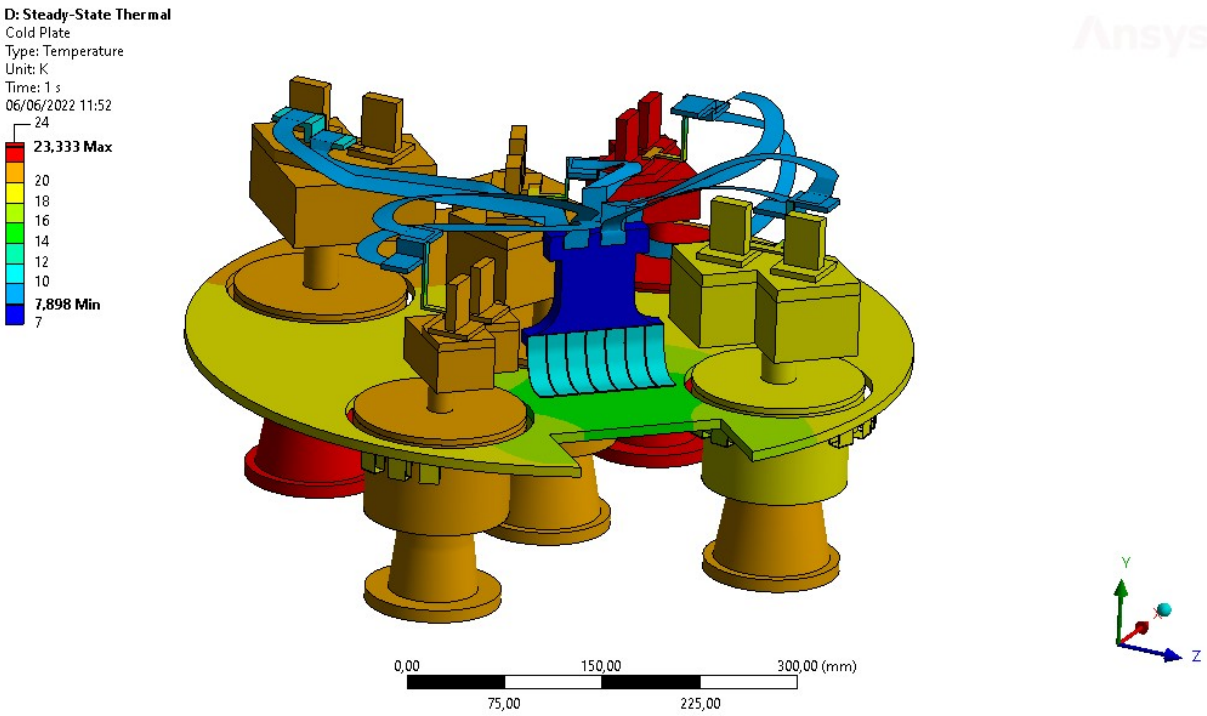

Figure 14: Temperature distribution at the second stage, obtained by a steady-state FEM thermal analysis.

passes through the rotary joint of the telescope and to a ground based SSD harddisk array. The data is directly stored here. An acquisition computer is used for post processing and further reduction of the data. The output is sent to be stored on a secure central disk array in the IAC computing centre.

6. CONCLUSIONS

We have presented the new MFI2 instrument for the QUIJOTE project. The idea and scientific motive behind the instrument has been described as well as the theoretical implementation and resulting improvements over the old MFI design. The status of the project is clearly seen showing the advanced cryogenic implementation. The FPGA and accompanying down converter is under development following a clear design scheme. MFI2 is expected to be installed in the focal plane of the first QUIJOTE telescope (QT-1) in the second half of 2022. Commissioning of the MFI2 will take place in the following few months, then followed by scientific operations.

ACKNOWLEDGMENTS

The MFI2 instrument is being developed by the Instituto de Astrofisica de Canarias (IAC), with an instrumental participation from the Universidad Politecnica de Cartagena (UPCT). Partial financial support is provided by the Spanish Ministry of Science and Innovation (MICINN), under the projects AYA2017-84185-P, IACA15-BE-3707, EQC2018-004918-P and the FEDER Agreement INSIDE-OOCC (ICTS-2019-03-IAC-12). We also acknowledge financial support of the Severo Ochoa Programs SEV-2015-0548 and CEX2019-000920-S. The *QUIJOTE* experiment is being developed by the Instituto de Astrofisica de Canarias (IAC), the Instituto de Fisica de Cantabria (IFCA), and the Universities of Cantabria, Manchester and Cambridge. We acknowledge the use of the Legacy Archive for Microwave Background Data Analysis (LAMBDA), part of the High Energy Astrophysics Science Archive Center (HEASARC). HEASARC/LAMBDA is a service of the Astrophysics Science Division at the NASA Goddard Space Flight Center.

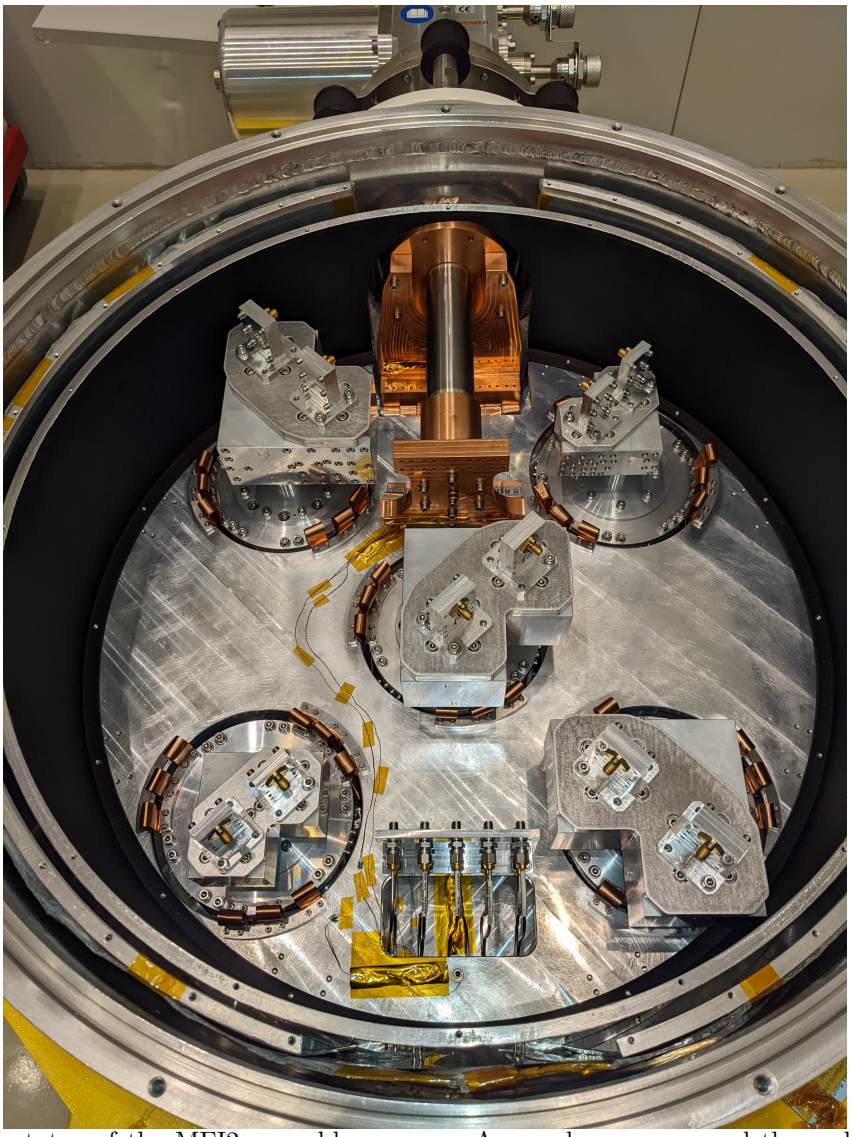

Figure 15: Current status of the MFI2 assembly process. As can be seen, several thermal sensors have been placed over the plate. There will be three sensors per plate to monitor the temperature distribution (one of them directly attached to the thermal link of the cryocooler). There is also a sensor on each of the ultra-LNAs.

References

[1] Rubiño-Martín, J. A., Rebolo, R., Aguiar, M., Génova-Santos, R., Gómez-Reñasco, F., Herreros, J. M., Hoyland, R. J., et al., "The QUIJOTE-CMB experiment: studying the polarisation of the galactic and cosmological microwave emissions," in [*Ground-based and Airborne Telescopes IV*], *Society of Photo-Optical Instrumentation Engineers (SPIE) Conference Series* **8444**, 84442Y (Sept. 2012).

[2] Hoyland, R. J. et al, "The status of the QUIJOTE multi-frequency instrument ," in [*Millimeter, Submillimeter, and Far-Infrared Detectors and Instrumentation for Astronomy VI*], *Society of Photo-Optical Instrumentation Engineers (SPIE) Conference Series* **8452**, 85233 (Sept. 2012).

[3] Rubiño-Martín, J. A., Rebolo, R., Aguiar, M., Génova-Santos, R., Gómez-Reñasco, F., Herreros, J. M., Hoyland, R. J., López-Caraballo, C., Pelaez Santos, A. E., Sanchez de la Rosa, V., Vega-Moreno, A., Viera-Curbelo, T., Martínez-Gonzalez, E., Barreiro, R. B., Casas, F. J., Diego, J. M., Fernández-Cobos,

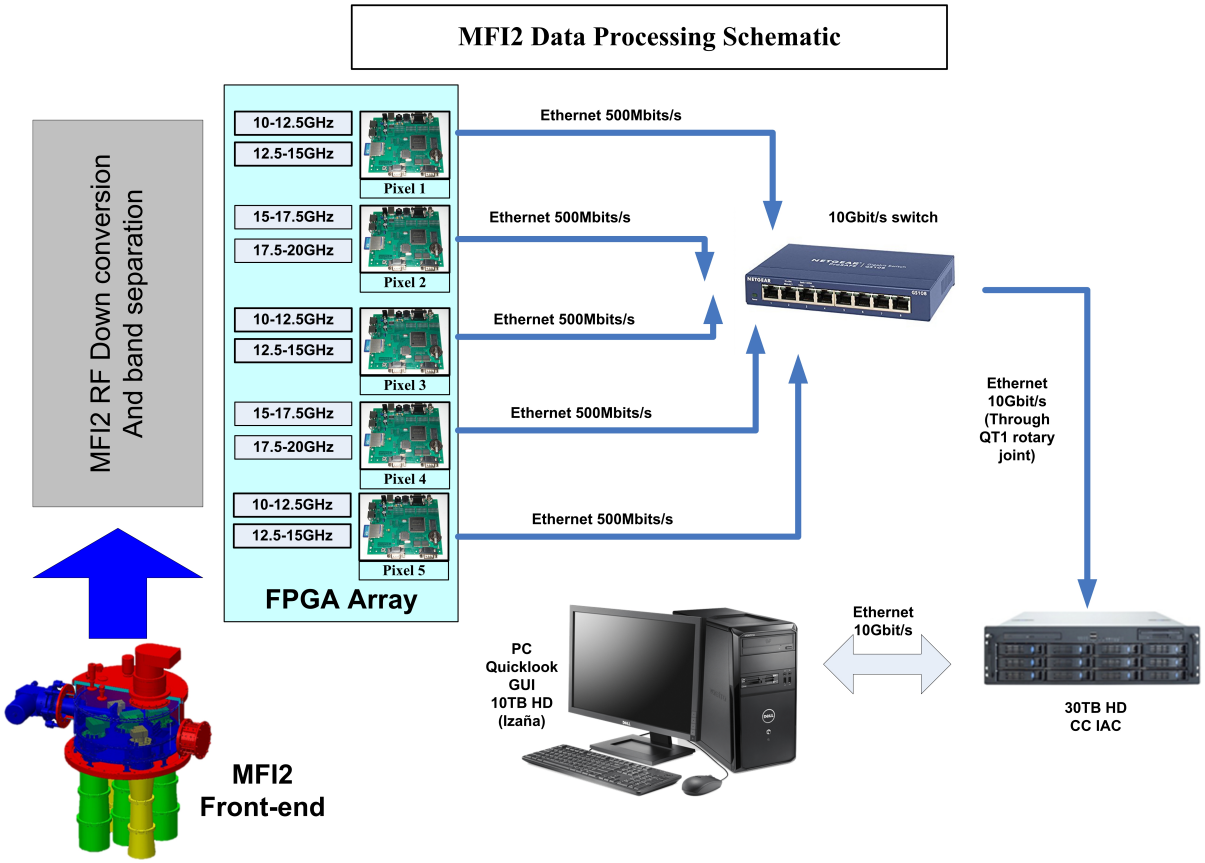

Figure 16: The MFI2 data processing schematic showing the signal and data flow through the acquisition process. The flow starts at the cryogenically cooled MFI2 instrument and ends in the storage SSD harddisks.

R., Herranz, D., López-Caniego, M., Ortiz, D., Vielva, P., Artal, E., Aja, B., Cagigas, J., Cano, J. L., de la Fuente, L., Mediavilla, A., Terán, J. V., Villa, E., Piccirillo, L., Battye, R., Blackhurst, E., Brown, M., Davies, R. D., Davis, R. J., Dickinson, C., Harper, S., Maffei, B., McCulloch, M., Melhuish, S., Pisano, G., Watson, R. A., Hobson, M., Grainge, K., Lasenby, A., Saunders, R., and Scott, P., "The QUIJOTE-CMB experiment: studying the polarisation of the galactic and cosmological microwave emissions," in [*Ground-based and Airborne Telescopes IV*], **8444**, 84442Y (Sept. 2012).

[4] Gomez, A., Murga, G., Etxeita, B., Sanquirce, R., Rebolo, R., Rubiño-Martin, J. A., Herreros, J.-M., Hoyland, R., Gomez, F., Génova-Santos, R. T., Piccirillo, L., Maffei, B., and Watson, R., "QUIJOTE telescope design and fabrication," in [*Ground-based and Airborne Telescopes III*], **7733**, 77330Z (July 2010).

[5] Sanquirce, R., Etxeita, B., Murga, G., Fernandez, E., Sainz, I., Sánchez, V., Viera-Curbelo, T. A., Gómez, M. F., Aguiar-Gonzalez, M., Hoyland, R. J., Pérez de Taoro, Á. R., Vega, A., Rebolo-López, R., and Rubiño, J. A., "A 200-GHz telescope unit for the QUIJOTE CMB Experiment," in [*Ground-based and Airborne Telescopes V*], **9145**, 914524 (July 2014).

[6] Sanquirce-García, R., Sainz-Pardo, I., Etxeita-Arriaga, B., Murga-Llano, G., Fernandez-Santos, E., Sánchez-de-la-Rosa, V., Viera-Curbelo, T. A., Gómez-Reñasco, F., Aguiar-González, M., Pérez de Taoro, M. R., and Rubiño-Martín, J. A., "Final acceptance of the 200 GHz telescope unit for the QUIJOTE CMB experiment," in [*Ground-based and Airborne Telescopes VI*], **9906**, 99064N (July 2016).

[7] Pérez-de-Taoro, M. R., Aguiar-González, M., Cózar-Castellano, J., Génova-Santos, R., Gómez-Reñasco, F., Hoyland, R., Peláez-Santos, A., Poidevin, F., Tramonte, D., Rebolo-López, R., Rubiño-Martín, J. A., Sánchez-de-la-Rosa, V., Vega-Moreno, A., Viera-Curbelo, T., Vignaga, R., Casas, F. J., Martinez-Gonzalez, E., Ortiz, D., Aja, B., Artal, E., Cano-de-Diego, J. L., de-la-Fuente, L., Mediavilla, A., Terán, J. V., Villa, E., Harper, S., McCulloch, M., Melhuish, S., Piccirillo, L., and Lasenby, A., "QUIJOTE Experiment: status of telescopes and instrumentation," in [*Ground-based and Airborne Telescopes VI*], **9906**, 99061K (July 2016).

[8] Fasano, A., Aguiar, M., Benoit, A., Bideaud, A., Bourrion, O., Calvo, M., Catalano, A., de Taoro, A. P., Garde, G., Gomez, A., Gomez Renasco, M. F., Goupy, J., Hoarau, J., Hoyland, R., Macías-Pérez, J. F., Marpaud, J., Monfardini, A., Pisano, G., Ponthieu, N., Rubiño Martín, J. A., Tourres, D., Tucker, C., Beelen, A., Bres, G., De Petris, M., de Bernardis, P., Lagache, G., Lamagna, L., Luzzi, G., Marton, M., Masi, S., Rebolo, R., and Roudier, S., "The KISS Experiment," *Low Temperature Physics* **199**, 529–536 (Dec. 2020).

[9] Castro-Almazán, J. A., Muñoz-Tuñón, C., García-Lorenzo, B., Pérez-Jordán, G., Varela, A. M., and Romero, I., "Precipitable Water Vapour at the Canarian Observatories (Teide and Roque de los Muchachos) from routine GPS," *Observatory Operations: Strategies, Processes, and Systems VI* **9910**(May), 99100P (2016).

[10] Honda, S., Choi, J., Génova-Santos, R. T., Hattori, M., Hazumi, M., Ikemitsu, T., Ishida, H., Ishitsuka, H., Jo, Y., Karatsu, K., Kiuchi, K., Komine, J., Koyano, R., Kutsuma, H., Lee, K., Mima, S., Minowa, M., Moon, J., Nagai, M., Nagasaki, T., Naruse, M., Oguri, S., Otani, C., Peel, M., Rebolo-López, R., Rubiño-Martín, J. A., Sekimoto, Y., Sueno, Y., Suzuki, J., Taino, T., Tajima, O., Tomita, N., Tsuji, Y., Uchida, T., Won, E., and Yoshida, M., "On-site performance of GroundBIRD, a CMB polarization telescope for large angular scale observations," in [*Ground-based and Airborne Telescopes VIII*], Marshall, H. K., Spyromilio, J., and Usuda, T., eds., **11445**, 1379 – 1386, International Society for Optics and Photonics, SPIE (2020).

[11] Addamo, G., Ade, P. A. R., Baccigalupi, C., Baldini, A. M., Battaglia, P. M., Battistelli, E. S., Baù, A., de Bernardis, P., Bersanelli, M., Biasotti, M., Boscaleri, A., Caccianiga, B., Caprioli, S., Cavaliere, F., Cei, F., Cleary, K. A., Columbro, F., Coppi, G., Coppolecchia, A., Cuttaia, F., D'Alessandro, G., De Gasperis, G., De Petris, M., Fafone, V., Farsian, F., Ferrari Barusso, L., Fontanelli, F., Franceschet, C., Gaier, T. C., Galli, L., Gatti, F., Genova-Santos, R., Gerbino, M., Gervasi, M., Ghigna, T., Grosso, D., Gruppuso, A., Gualtieri, R., Incardona, F., Jones, M. E., Kangaslahti, P., Krachmalnicoff, N., Lamagna, L., Lattanzi, M., López-Caraballo, C. H., Lumia, M., Mainini, R., Maino, D., Mandelli, S., Maris, M., Masi, S., Matarrese, S., May, A., Mele, L., Mena, P., Mennella, A., Molina, R., Molinari, D., Morgante, G., Natale, U., Nati, F., Natoli, P., Pagano, L., Paiella, A., Panico, F., Paonessa, F., Paradiso, S., Passerini, A., Perez-de-Taoro, M., Peverini, O. A., Pezzotta, F., Piacentini, F., Piccirillo, L., Pisano, G., Polenta, G., Poletti, D., Presta, G., Realini, S., Reyes, N., Rocchi, A., Rubino-Martin, J. A., Sandri, M., Sartor, S., Schillaci, A., Signorelli, G., Siri, B., Soria, M., Spinella, F., Tapia, V., Tartari, A., Taylor, A. C., Terenzi, L., Tomasi, M., Tommasi, E., Tucker, C., Vaccaro, D., Vigano, D. M., Villa, F., Virone, G., Vittorio, N., Volpe, A., Watkins, R. E. J., Zacchei, A., Zannoni, M., and LSPE Collaboration, "The large scale polarization explorer (LSPE) for CMB measurements: performance forecast," **2021**, 008 (Aug. 2021).

[12] Rubiño Martín, J. A., Alonso Arias, P., Hoyland, R. J., Aguiar-González, M., De Miguel-Hernández, J., Génova-Santos, R. T., Gomez-Reñasco, M. F., Guidi, F., Fernández-Izquierdo, P., Fernández-Torreiro, M., Fuerte-Rodriguez, P. A., Hernandez-Monteagudo, C., López-Caraballo, C. H., Perez-de-Taoro, A., Peel, M. W., Rebolo, R., Zamora-Jimenez, A., González-Carretero, E. D., Colodro-Conde, C., Pérez-Lemus, C., Toledo-Moreo, R., Pérez-Lizán, D., Cuttaia, F., Terenzi, L., Franceschet, C., Realini, S., Chluba, J., Murga-Llano, G., and Sanquirce-Garcia, R., "The Tenerife Microwave Spectrometer (TMS) experiment: studying the absolute spectrum of the sky emission in the 10-20GHz range," in [*Society of Photo-Optical Instrumentation Engineers (SPIE) Conference Series*], *Society of Photo-Optical Instrumentation Engineers (SPIE) Conference Series* **11453**, 114530T (Dec. 2020).

[13] Hinshaw, G., Larson, D., Komatsu, E., Spergel, D. N., Bennett, C. L., Dunkley, J., Nolta, M. R., Halpern, M., Hill, R. S., Odegard, N., Page, L., Smith, K. M., Weiland, J. L., Gold, B., Jarosik, N., Kogut, A.,

Limon, M., Meyer, S. S., Tucker, G. S., Wollack, E., and Wright, E. L., "Nine-year Wilkinson Microwave Anisotropy Probe (WMAP) Observations: Cosmological Parameter Results," **208**, 19 (Oct. 2013).

[14] Planck Collaboration, Aghanim, N., Akrami, Y., Ashdown, M., Aumont, J., et al., "Planck 2018 results. VI. Cosmological parameters," **641**, A6 (Sept. 2020).

[15] Rubiño-Martín, J. A. et al., "*QUIJOTE* scientific results - IV. A northern sky survey at 10–20 GHz with the Multi-Frequency Instrument," *, in prep.* (2022).

[16] Peacock, J. A., Schneider, P., Efstathiou, G., Ellis, J. R., Leibundgut, B., Lilly, S. J., and Mellier, Y., "ESA-ESO Working Group on "Fundamental Cosmology"." "ESA-ESO Working Group on "Fundamental Cosmology", Edited by J.A. Peacock et al. ESA, 2006." (Oct. 2006).

[17] Krachmalnicoff, N., Carretti, E., Baccigalupi, C., Bernardi, G., Brown, S., Gaensler, B. M., Haverkorn, M., Kesteven, M., Perrotta, F., Poppi, S., and Staveley-Smith, L., "S-PASS view of polarized Galactic synchrotron at 2.3 GHz as a contaminant to CMB observations," **618**, A166 (Oct. 2018).

[18] Price, D. C., "Spectrometers and Polyphase Filterbanks in Radio Astronomy," *arXiv e-prints* , arXiv:1607.03579 (July 2016).